METHODOLOGY



Contact Stiffness and Damping in Atomic-Scale Friction: An Approximate Estimation from Molecular Dynamics Simulations

Gunan Zhang¹ · Rong-Guang Xu¹ · Yuan Xiang¹ · Yongsheng Leng¹

Received: 6 November 2023 / Accepted: 17 December 2023 / Published online: 17 January 2024 © The Author(s), under exclusive licence to Springer Science+Business Media, LLC, part of Springer Nature 2024

Abstract

The stick—slip friction observed in an atomic force microscope (AFM) experiment has been widely studied using the Prandtl-Tomlinson (PT) model or molecular dynamics (MD) simulations. However, the mechanisms of friction energy dissipation in AFM are still not well understood. Our detailed MD simulations of a benchmark system, a Pt metal tip sliding on the Au (111) surface, provide a method of computing the contact stiffness and damping between the tip apex and the metal surface. We revealed that the contact stiffness is largely dependent on the *very first contact layer atoms* of the tip apex, but essentially independent of the temperature and the atomic mass of the AFM tip, and is also less dependent on the normal load if the contact geometry remains unchanged in elastic contact. Furthermore, by connecting the atomic relaxation rate to the damping coefficient, an important parameter gauging the friction dissipation in the PT model but the choice of which is usually empirical, we demonstrate that this damping coefficient is dependent on the atomic structure of the tip apex and the intrinsic relaxation rate of the individual atoms in the contact layer. We use such mechanisms to calculate the two parameters and carry out Langevin dynamics simulation within the framework of the PT model for two friction systems: a small Pt tip consisting of 3956 Pt atoms and a large polycrystalline Pt tip consisting of 18,365 Pt atoms. Our simulation results show that both tip apexes are *underdamped* in a stick—slip friction. We also demonstrate that the results from the Langevin dynamics simulation using these two critical parameters compared remarkably well with the straightforward MD simulation results in a range of sliding velocity (V = 0.01 - 1 m/s).

Keywords Atomic-scale friction · Energy dissipation · Stick-slip motion · Molecular dynmics · Contact stiffness · Damping

1 Introduction

Atomic force microscope (AFM) has been widely used as a foundational tool to study atomic-scale or nanoscale friction of a variety of materials [1–6], including recently emerging 2D layered materials due to their unusual structural lubricity [7–10]. Since its invention [11], the high-resolution imaging capability of the AFM in the contact mode has dramatically impacted various areas in nanotechnology, materials science, biology, and broad surface and interface science. This achievement was largely attributed to the probe tip well-defined, stick—slip friction signals with an atomic resolution. The intrinsic stick—slip friction dynamics in AFM

Traditionally, the stick-slip friction in AFM has been described by the Prandtl-Tomlinson (PT) model [19, 20]. Here, an AFM model tip with a single point mass is driven by an effective linear spring to slide on a periodic sinusoidal potential. This potential represents the interaction between



also attracted tremendous interest in theoretical modeling and computer simulations to fundamentally understand the origin of friction and energy dissipation mechanisms [3–6, 12–17]. By scanning a sample surface using an AFM probe tip, which is often prepared by thermally evaporating a metal coating on a silicon cantilever [16], or simply using an amorphous material such as a silicon tip with its oxide (SiO₂) on the tip apex [17, 18], or a silicon nitride (Si₃N₄) tip [9], one can directly measure the friction forces between the probe tip and the sample surface. Modeling the tip-substrate friction to fully understand the energy dissipation mechanism of nanoscale friction requires careful thinking of the molecular model that should reflect the key features of the AFM experimental setting.

Yongsheng Leng leng@gwu.edu

Department of Mechanical and Aerospace Engineering, The George Washington University, Washington, DC 20052, USA

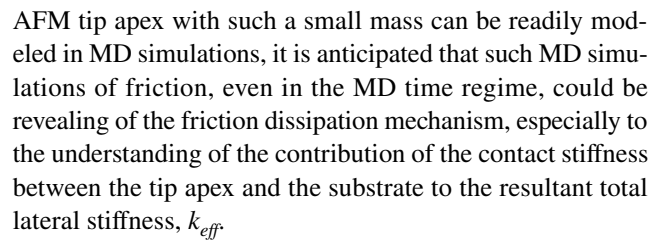
the tip and the crystalline substrate. The amplitude of the periodic corrugation potential should be properly chosen to reflect the actual AFM loading condition [4]. When simulating the friction *dynamics* with the thermal effect being considered within the framework of the PT model, a damping term and a thermal random force are usually included to the tip motion in the relevant Langevin equation [4]. However, the origin of this damping (more precisely, the intrinsic friction dissipation) cannot be retrieved from the PT model itself [14, 15].

Direct molecular dynamics (MD) simulations using optimally matched AFM friction parameters were reported previously [16, 17]. These optimal parameters include the effective lateral spring stiffness, the contact area, and the normal load. Nevertheless, the sliding speeds in MD simulations are still many orders of magnitude higher than those in AFM experiments due to the well-known timescale issue. Further, the actual contribution of the contact stiffness of the tip-substrate contact to the total effective lateral spring stiffness in AFM is usually unknown or has not been well calibrated [21].

In this paper we carried out straightforward MD simulations to directly calculate the contact stiffness and damping of a benchmark system, a Pt model tip sliding on the Au (111) surface. Our findings demonstrate that the contact stiffness is largely determined by the *very first* contact layer atoms in the tip apex, while the damping coefficient can be calculated based on the linear scaling of dissipation rate of the contact layer atoms according to Krylov et al. [15] We showed that other factors such as the temperature, tip mass, and normal load have less effect on these two terms.

2 Theoretical Consideration of the PT Model

It is well recognized that in AFM friction measurements, the total effective lateral stiffness, $k_{\it eff}$, of the AFM cantilever-tip assembly in contact with a sample substrate, is determined not only by the torsional bending stiffness of the cantilever, k_T , but also by the lateral contact stiffness of the AFM tip – substrate contact, k_{cont} [12, 16, 21]. In general, k_{eff} can be readily calibrated from the slope of the stick-slip friction in the sticking stage. Theoretical modeling by Krylov et al. [13–15] on the friction energy dissipation in AFM suggested that the ultrafast dynamics of the AFM tip apex, which has an extremely small mass in the range of $10^{-23} - 10^{-20}$ kg (corresponding to a few hundred to a few hundred thousand atomic particles in the tip apex), is largely responsible for the friction dissipation. They proposed a two-mass-two-spring (2*m*2*s*) friction model [14] to simulate stick–slip friction in AFM, in which the tip apex was represented by an extremely small mass m, while the rest of the tip body and cantilever took a lumped mass in the order of 10^{-11} kg. Given that the



In general, k_{eff} can be considered as a combination of the following mechanical springs in sequential connection:

$$\frac{1}{k_{eff}} = \frac{1}{k_{cont}} + \frac{1}{k_{tip}} + \frac{1}{k_T} \tag{1}$$

Here, k_{tip} is the AFM tip bending spring constant considering its 6–10 µm in length at the end of the AFM cantilever, which was usually not included when calibrating the cantilever torsional bending stiffness, k_T [22], while k_{cont} is understood as the lateral contact stiffness of the tip apexsubstrate contact.

For the friction dynamics of an AFM tip apex *alone*, the simple one-mass PT model [19, 20] is still available to be used to describe the stick–slip sliding friction [4]. Here, the tip apex with its mass m, is driven by an equivalent spring k, given by $1/k = 1/k_{tip} + 1/k_T$, over an effective potential

$$V(x,t) = -\frac{E_0}{2}\cos\left(\frac{2\pi x}{a}\right) + \frac{1}{2}k(Vt - x)^2$$
 (2)

where E_0 is the amplitude of the periodic corrugation potential induced by substrate and is dependent on the normal load. Parameter a is the lattice constant of the substrate, and V is the AFM cantilever scanning velocity. Friction dynamics of the tip apex motion x = x(t) in the thermal PT model can be described in the Langevin equation, viz [4]

$$m\ddot{x} + m\gamma\dot{x} + k(x - Vt) = -\frac{\partial V_{\text{int}}(x, t)}{\partial x} + \xi(t)$$
 (3)

Here, when the damping coefficient γ (in the unit of s⁻¹) reaches the critical damping value, i.e., $\gamma = \gamma_c = 2\sqrt{k/m}$, or the damping ratio $\zeta = \gamma/\gamma_c = 1$, the friction system will be critically damped. On the right of Eq. (3), V_{int} is the tip–substrate interaction potential, and $\xi(t)$ is the random thermal activation force, satisfying the fluctuation–dissipation theorem, with its zero mean $\langle \xi(t) \rangle = 0$ and δ correlated [4], i.e. $\langle \xi(t)\xi(t') \rangle = 2m\gamma k_B T \delta(t-t')$, where k_B is the Boltzmann constant and T is the temperature. The random force and the damping term in Eq. (3) arise from the interactions between the model tip and the substrate in the form of phonons and/or other fast excitations that are not treated explicitly [4]. We note that recent studies showed that the origin of this damping term is directly related to the dephasing of phonons that are generated in the slip process [23].

In AFM friction measurements, the effective lateral stiffness, k_{eff} , is readily obtained from the slope of stick-slip



Tribology Letters (2024) 72:24 Page 3 of 10 **2**

friction in the sticking stage [12, 16, 24]. If the lateral contact stiffness, k_{cont} , between the AFM tip apex and the substrate can be properly calculated from MD simulations, then one can simply determine the equivalent spring k in the PT model based on Eq. (1), without the need to calibrate k_{tip} and k_T , i.e.

$$1/k = 1/k_{eff} - 1/k_{cont} (4)$$

One should keep in mind that the driving spring, k, in the Langevin Eq. (3), is slightly larger than k_{eff} . This is because k_{eff} is the derivative of the measured stick—slip lateral force in the sticking part with respect to the driving support position, Vt. This measured lateral force, usually called the stick—slip friction force, is defined as F = k(Vt - x) according to Eq. (3). Thus, we have

$$k_{eff} = dF/d(Vt) = k(1 - \dot{x}/V) \tag{5}$$

It is worth noting that even in the sticking stage, the instantaneous tip velocity \dot{x} is not necessarily equal to zero. From Eqs. (4) and (5), one finds that the tip velocity \dot{x} is given by

$$\dot{x} = \frac{k_{eff}}{k_{cont}}V \tag{6}$$

Here, \dot{x} should be understood as the *instantaneous* tip velocity due to the entire modeling in the MD time regime. There is a distinction between this variable and the

thermodynamic average value in the 2m2s friction model [14], where a colossal cantilever dynamics is involved. In the following discussion through MD simulations, we will show that the contact stiffness, k_{cont} is much larger than k_{eff} .

3 Molecular Dynamics Simulation Benchmark System

In this section we consider direct MD simulation of a Pt metal tip apex sliding on the Au (111) surface. This is a well-studied benchmark system in AFM atomic-scale friction experiments [16] and in MD simulations [16, 25]. Two friction models are considered here, as shown in Fig. 1. The first is a small single crystalline Pt tip sliding on the Au (111) surface, and the second is a large polycrystalline Pt tip with $R \approx 10$ nm in radius that has a single crystalline protrusion in contact with an Au (111) substrate. The detailed preparation for the large Pt tip apex in contact with the Au (111) surface has been described in our previous publication [25], while the preparation for the small Pt tip contact system follows the similar procedure. The small Pt tip has 3956 Pt atoms (defined as the Pt₃₉₅₆), plus 9 Au atoms attached onto the first contact layer and additional 4 Au atoms attached onto the second layer of the Pt₃₉₅₆ tip due to adhesion. The large polycrystalline Pt tip contains 18,365 Pt atoms (defined as the Pt₁₈₃₆₅), plus 111 Au atoms attached onto the first

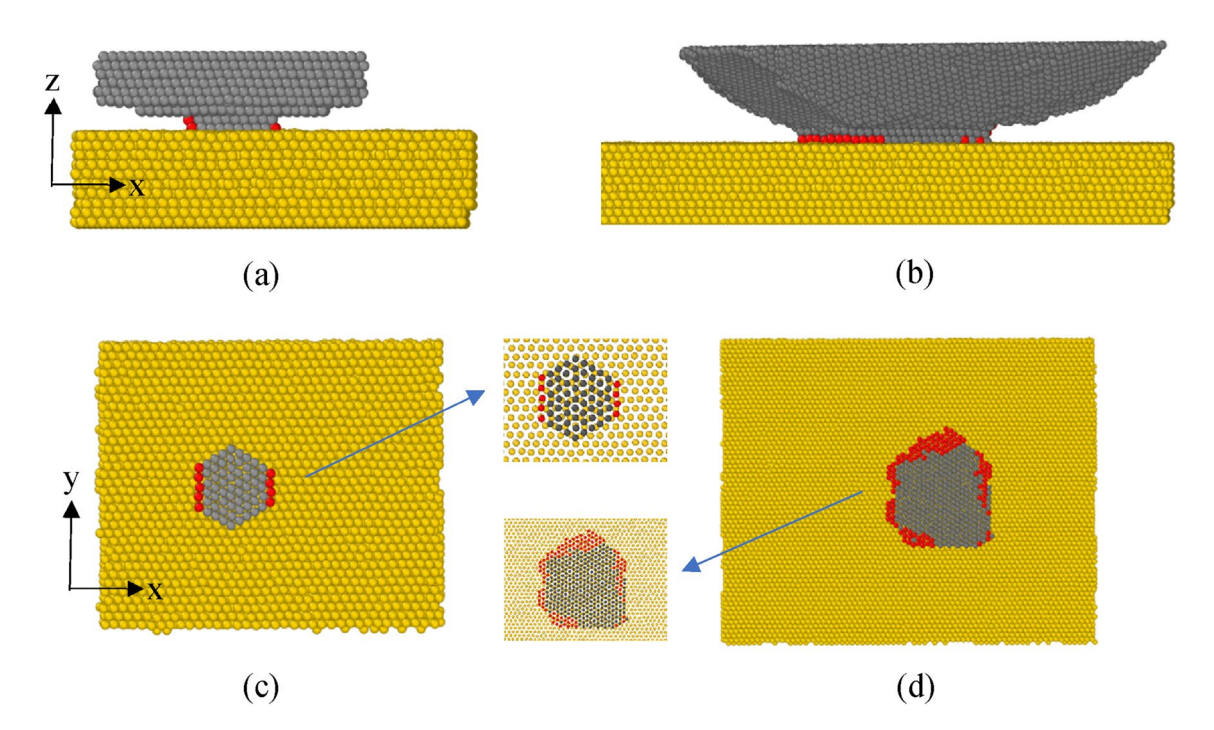


Fig. 1 Pt-Au (111) friction models. The side views $\bf a$ and $\bf b$ show the full atomic settings of the Pt₃₉₅₆ and Pt₁₈₃₆₅ tip apexes in contact with the Au (111) surface. The top views $\bf c$ and $\bf d$ show the first contact layer of the Pt tip apexes, including the attached gold atoms (shown

in red color) in contact with the first Au (111) layer. The insets between ${\bf c}$ and ${\bf d}$ show the Moiré contact pattern between the Pt tip apex and the Au (111) surface



contact layer and additional 7 gold atoms attached onto the second and the third layers of the single crystalline Pt protrusion [25] (Fig. 1). Table 1 shows the relevant atom numbers associated with the two Pt tip apexes and their tip masses.

In MD simulations, initial stable contacts between the tip apexes and the Au (111) surface were achieved upon a self-adjusted Moiré contact pattern was formed (see the inset in Fig. 1) [25]. The Pt tip apex is then connected to a driven block using a driving spring, k, along the x-direction. According to Eq. (5), k should be slightly larger than $k_{eff} = 6$ N/m, as calibrated in AFM friction measurements [16]. Consequently, we choose k = 7.8 N/m and 7.1 N/m for the Pt₃₀₅₆ and Pt₁₈₃₆₅ tip apexes, respectively. In addition, considering the restriction of the tip movement along the longitudinal direction of the cantilever, a more rigid spring with an arbitrary value of 300 N/m is applied along the y-direction. A normal force of 0.6 nN, consistent with the load in AFM friction measurements [16], is applied to the top-rigid-layer atoms of the Pt tip apex. Periodic boundary conditions are applied in the x- and y-directions during the friction simulation runs. Interatomic interactions are described by the embedded atom method (EAM) potential [26]. The time step of 2.0 fs has been used throughout MD simulations using the LAMMPS package [27, 28], while the temperature of the system in MD simulations is controlled at 293 K by the Nosé–Hoover thermostat [29].

4 Results and Discussion

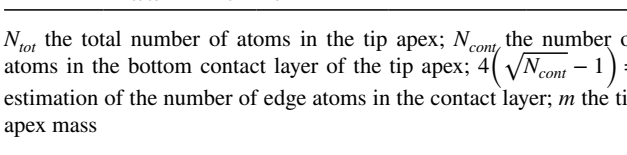
4.1 Contact Stiffness k_{cont}

We first demonstrate that the contact stiffness between the Pt tip apex and the Au (111) surface k_{cont} , depends on the detailed atomic structure of the tip apex and varies slightly with the normal load, but is largely independent of temperature and the tip atomic mass. We begin with the first investigation of the small Pt tip apex, the Pt₃₉₅₆ that contains 3956 Pt atoms and 13 attached Au atoms (Table 1). In our previous study [25], we showed that in MD time regime, the stick-slip friction of an AFM model

Table 1 The relevant atom numbers associated with the two Pt tip apexes

	N_{tot}	N_{cont}	$4\left(\sqrt{N_{cont}}-\right.$	$(1)^m (10^{-21} \text{ kg})$
Small tip	Pt ₃₉₅₆ + Au ₁₃	Pt ₅₆ + Au ₉	28 (25)	1.29
Large tip	$Pt_{18365} + Au_{118}$	$Pt_{342} + Au_{111}$	81 (80)	6.02

 N_{tot} the total number of atoms in the tip apex; N_{cont} the number of atoms in the bottom contact layer of the tip apex; $4\left(\sqrt{N_{cont}}-1\right)=$ estimation of the number of edge atoms in the contact layer; m the tip



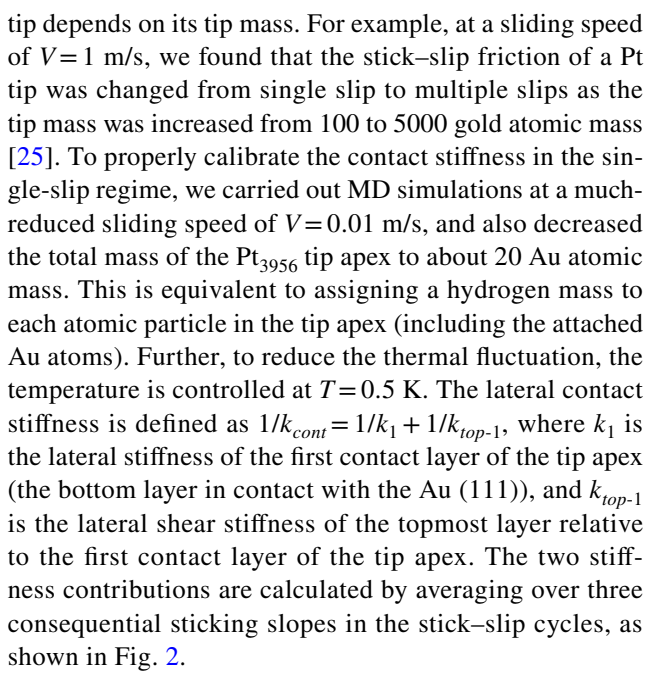


Figure 2a shows the variation of the stick-slip friction force under a normal load of 0.6 nN within an initial 8 Å sliding distance. The variation of the actual position of the tip apex versus the sliding distance of the driven block is also shown in the figure. The driving spring used is k=7.8N/m, resulting in an effective lateral stiffness close to k_{eff} =6 N/m, as calibrated in AMF friction measurements [16]. In Fig. 2b and c, we plot the variations of the same lateral friction force versus the *center-of-mass* (COM) sliding distance of the bottom contact layer of the tip apex, as well as versus the shear deformation of the topmost layer of the tip apex relative to its bottom contact layer. This COM sliding distance of the bottom contact layer represents the combined actual shear deformation of the tip apex bottom layer and the gold substrate during the sticking stage. k_1 and k_{top-1} are simply the slopes of these two shear deformation curves in the sticking stage. The contact stiffness is then calculated according to the relation $1/k_{cont} = 1/k_1 + 1/k_{top-1}$, as shown in Table 2.

To investigate the temperature effect on the contact stiffness, in Fig. 2d –f, we plot the friction force variations at T=293 K (the green stick–slip friction curve). It is seen that the relevant force slopes have almost no changes, except the large thermal fluctuations and early slips due to the effect of thermal activations.

We have also investigated the friction dynamics of the Pt_{3956} tip apex at the low temperature of T = 0.5 K when the actual atomic masses of Pt (= 195 amu) and Au (= 197 amu) are used at the sliding speed of V=0.01 m/s (see Fig. 2d –f the red stick-slip friction curve). Except for large force oscillations due to the system being underdamped (see below discussion), all the slopes of friction force versus distance/shear deformation in the sticking stages are essentially unchanged.



Tribology Letters (2024) 72:24 Page 5 of 10 **2**

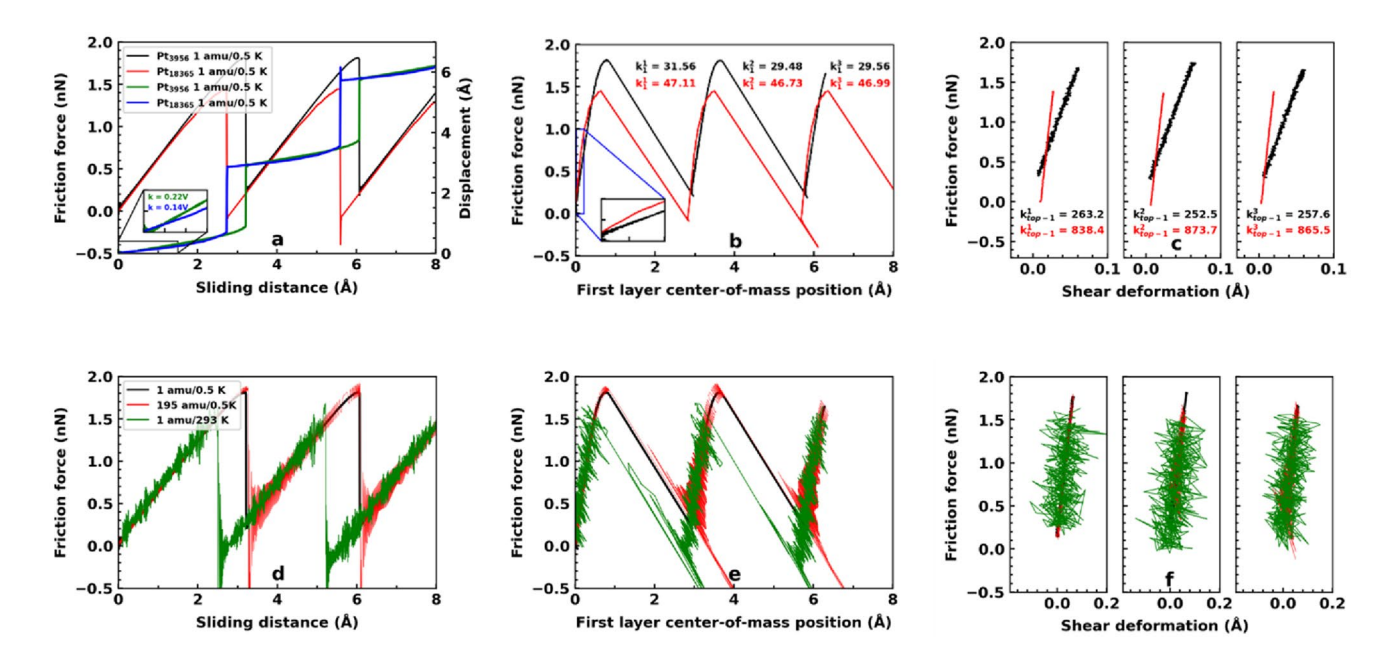


Fig. 2 Variations of the stick–slip friction force of the Pt_{3956} and Pt_{18365} tip apexes at T=0.5 K and V=0.01 m/s, versus **a** the sliding distance, **b** the center-of-mass position of the bottom contact layer, and **c** the shear deformation of the topmost layer relative to the bottom contact layer of the tip apex. The variation of the actual position of the tip apex versus the sliding distance is also shown in panel (**a**), where the inset shows at the sticking stage the slopes of the two tip

apexes positions versus the sliding distance. The inset in **b** shows the difference in slope at the sticking stage for the two different tip apexes (Pt₃₉₅₆ and Pt₁₈₃₆₅). Values of k_1 and k_{lop-1} corresponding to the three sticking stages are also depicted in (**b**) and (**c**), whose average values are given in Table 2. **d**-**f** show comparisons of MD simulation results of using actual atomic mass of the tip apex, as well as the results at T=293 K

Table 2 Summary of MD calculated contact stiffness versus the PT model predictions, as well as the dimensionless parameter η , for the Pt₃₉₅₆ and Pt₁₈₃₆₅ tip apexes in contact with the Au (111) surface

	k ₁ (N/m)	k _{top-1} (N/m)	k_{cont} (N/m)	k	$k_{cont\text{-}PT}$ (N/m)	η_{MD} $/\eta_{PT}$
Pt ₃₉₅₆	30.2	257.7	27.03	7.71	39.27	3.51 / 5.09
Pt ₁₈₃₆₅	46.9	859.2	44.47	6.94	30.50	6.41 / 4.39

The results presented above suggest that the contact stiffness of the Pt_{3956} only depends on the detailed atomic structure of the tip apex, while the temperature and atomic mass used in MD simulation have almost no effect on the results. Following this important finding, for the large tip apex Pt_{18365} that has a total of 453 atomic particles in the contact layer (see Table 1), we only focus on the MD simulations at T=0.5 K under the same normal load of 0.6 nN, with the hydrogen mass assigned to both Pt and Au atoms (equivalent to a 100-Au mass for the whole tip apex [25]). The driving spring used in MD simulation for this large tip apex is adjusted to k=7.1 N/m to achieve an effective lateral stiffness close to k_eff=6 N/m. The results are also shown in Fig. 2a—c to compare with the Pt_{3956} results at the same sliding speed of V=0.01 m/s.

Comparative studies show that the maximum friction force for the Pt₁₈₃₆₅ tip apex is reduced to 1.4 nN under the same load of 0.6 nN, as compared to the 1.8 nN maximum

friction force for the Pt₃₉₅₆ tip apex (see Fig. 2a -c). The contact layer stiffness, k_1 , is increased by about 50% compared to that of the Pt₃₉₅₆ result (see the enlarged inset in Fig. 2b). Further, the shear stiffness of the tip apex body, k_{top-1} , is more than three times the shear stiffness of the Pt₃₉₅₆ tip apex (Fig. 2c). The results for the two tip apex friction systems are summarized in Table 2. Here, we also list the equivalent driving spring constant, k, calculated according to Eq. (4). The two values are very close to k = 7.8 N/m and 7.1 N/m used in MD simulations for the Pt_{3956} and Pt_{18365} tip apexes. From the calculated k_{cont} shown in Table 2 and the same effective lateral stiffness k_{eff} =6 N/m for both Pt₃₉₅₆ and Pt₁₈₃₆₅, we calculate the instantaneous velocity according to Eq. (6) for both tip apexes at the sticking stage, yielding $\dot{x} = 0.22V$ and 0.14V, respectively. The results are remarkably consistent with the slopes of the tip apex positions at the sticking stage, as shown in Fig. 2a for the sliding speed of V = 0.01 m/s.



Surprisingly, Table 2 clearly shows that the contact stiffness, k_{cont} , is largely determined by the contact layer lateral stiffness, k_1 , because k_{top-1} is about one order of magnitude higher than k_1 . This is consistent with theoretical calculations by Krylov et al. [13], who showed that the effective stiffness of the tip is practically independent of the full length of the tip, but the very first contact layer of atoms. The implication from this result is that friction dissipation at a sliding interface is largely determined by the fast dynamics of the contact-layer atoms in the tip apex, an important corollary that needs further investigations.

To evaluate how the atomic-scale contact stiffness depends on load, we have further conducted MD simulations under different normal loads, ranging from 0.6 nN to 30 nN, to examine the changes in k_1 and k_{top-1} for both Pt₃₉₅₆ and Pt₁₈₃₆₅ tip apexes. The results are shown in Fig. 3. For the small Pt_{3956} tip apex, there is a *slight* increase in both k_1 and k_{top-1} as the normal load is increased, especially under high normal loads where severe deformation at the contact interface happens. For the large Pt_{18365} tip apex, both k_1 and k_{top-1} fluctuate within the range of the normal load investigated and appear less dependent on the normal load. This is largely attributed to the fact that the atomic configuration at the contact layer remains unchanged throughout the range of normal loads applied. In general, these results are consistent with prior AFM friction force measurements [24]. We therefore conclude that the contact stiffness between the Pt tip apex and the Au (111) substrate depends on the detailed atomic structure of the tip apex, especially the first contact layer stiffness of the tip apex, and slightly varies with the normal load, but is largely independent of temperature and the tip atomic mass. We emphasize that the contact stiffness

of the tip apex studied in this work is about 4 to 7 times the effective lateral stiffness k_{eff} (= 6 N/m). Such a high contact stiffness is mainly attributed to the blunt tip apex that has tens to hundreds of atoms in the contact area. According to Eq. (6), the high contact stiffness of a blunt tip apex makes the actual sliding speed of the tip apex in the *sticking stage* being much slower than the sliding speed of the driving support. This is clearly shown in Fig. 2a.

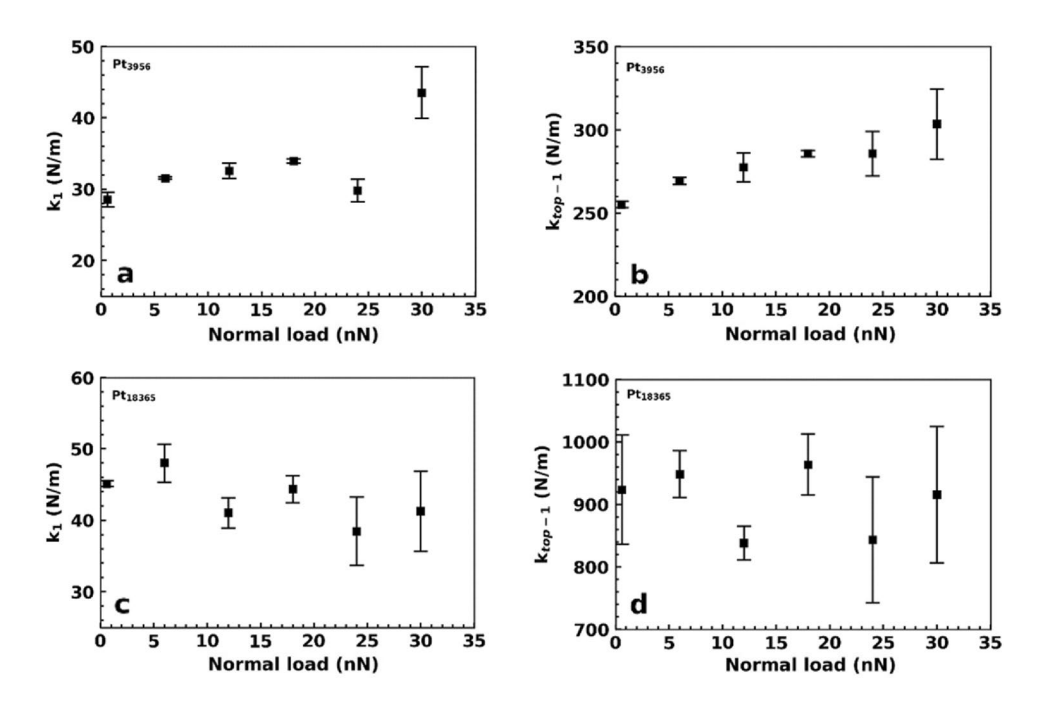
We now compare the contact stiffness (k_{cont}) directly obtained from the MD simulation with the stiffness of the tip-substrate potential according to the effective potential (2) in the PT model, given by [4, 24]

$$k_{cont-PT} = \frac{2\pi^2 E_0}{a^2} \tag{7}$$

Here, the amplitude of the periodic corrugation potential in Eq. (2), E_0 , is determined according to the linear relation between E_0 and the maximum friction force F_L^{max} , at zero temperature, given by [24] $E_0 = \frac{aF_L^{max}}{L}$. We choose a=0.288 nm, the first neighbor distance of the Au (111) surface. Values of F_L^{max} for both Pt₃₉₅₆ and Pt₁₈₃₆₅ tip apexes are determined from Fig. 2 as about 1.8 nN and 1.4 nN, respectively, yielding $E_0=1.03$ eV and 0.8 eV for the two tip apexes, separately.

As shown in Table 2, the contact stiffness predicted by the PT model for the Pt₃₉₅₆ tip apex overestimates the MD calculated value by about 45%, while that for the Pt₁₈₃₆₅ tip apex underestimates the stiffness by over 30%. Values of the dimensionless parameter η , which represents the ratio of the stiffness of the tip-substrate contact over that of the driving spring (for the PT model, $\eta = \frac{2\pi^2 E_0}{ka^2}$) [4, 24], are also

Fig. 3 Variations of the contact layer stiffness (k_1) and the shear stiffness (k_{top-1}) as a function of normal load for the small Pt_{3956} tip apex (panels **a** and **b**), and the large Pt_{18365} tip apex (panels **c** and **d**)





Tribology Letters (2024) 72:24 Page 7 of 10 **2**/

shown in Table 2 for the two tip apexes. While these η values are all greater than unity $(\eta > 1)$, a necessary condition for the occurrence of stick–slip friction as seen in Fig. 1, MD calculated values of η_{MD} indicate that Pt_{18365} tip apex has a more tendency to overshoot (a possibility of multiple slips [30]) during slips because of its much larger value of η_{MD} than that of the Pt_{3956} tip apex (see also Fig. 1 panels **a** and **b**). On the other hand, the PT model predicts that both tip apexes would have the similar probability of overshooting during friction slips.

4.2 Damping Coefficient y and Damping Ratio ζ

The damping coefficient (γ) in the Langevin Eq. (3) is a critical parameter in the thermal PT model [4] to properly describe the stick–slip friction dissipation in AFM. Recent studies by Krylov et al. on the origin of damping in atomic-scale friction suggested that the energy dissipation is relevant to the dephasing of phonons generated in the slip process [23]. Nearly critical damping of individual atoms has been confirmed based on a lattice dynamics calculation and MD simulation for a simple system [23]. In the following, we show a straightforward calculation from direct MD simulation results presented in 4.1.

For the tip apex – Au (111) contact shown in Fig. 1, following the nearly critical damping approximation of individual atoms in the contact layer [23], we know that the atomic dissipation rate takes a simple form [15]

$$\gamma_{at} \cong 2\sqrt{k_{at}m_{at}} \tag{8}$$

where m_{at} is the atomic mass and k_{at} is the lateral spring constant of individual atoms in the contact layer. Since the contact layer atoms in the tip apex experience approximately the same average friction dissipation rate γ_{at} due to the nearly critical damping approximation, one can calculate the total friction force, F_{diss} , which should be proportional to the contact area or the total number of atoms in the contact layer, i.e.

$$F_{diss} = N_{cont} \gamma_{at} \dot{x} \tag{9}$$

This simple linear scaling of dissipation rate was proved to be appropriate regardless of whether the atoms in the contact layer are considered as independent Einstein oscillators

Table 3 Summary of MD calculated lateral stiffness (k_{at}) of individual atoms in the contact layer, the damping coefficients γ , the dissipation rate $(m\gamma)$ in Langevin Eq. (3), and the damping ratio ζ , together

or coupled oscillators [23]. More sophisticated considerations involving the energy dissipation from the nearby tip atoms away from the contact interface and the phonon discrimination mechanism also reached the similar conclusion [15]. Therefore, it is the contact area, i.e., the number of atoms in the contact layer, N_{cont} , that determines how much mechanical energy is temporarily stored in the contact and subsequently dissipated into surrounding materials.

Since the dissipative friction force, $F_{\rm diss}$, is also relevant to the friction term in the Langevin Eq. (3), i.e., $F_{\rm diss} = m\gamma\dot{x}$, we can readily see that the dissipation rate in (3), $m\gamma$ (in the unit of kg s⁻¹), is only relevant to the total dissipation rate of the contact layer atoms, i.e., $m\gamma = 2N_{cont}\sqrt{k_{at}m_{at}}$. Such a simple relation also suggests that, if we consider that the attached Au atoms have approximately the same atomic mass as the Pt particles, then the damping coefficient γ , depends not only on the atomic number ratio N_{cont}/N_{tot} , a structure property of the tip apex, but also on the lateral vibration frequency of individual atoms in the contact layer $\sqrt{k_{at}/m_{at}}$, an intrinsic physical property of the friction system.

The average lateral stiffness of the individual atoms in the contact layer, k_{at} , can be calculated from the contact layer stiffness, k_1 , divided by the effective number of atoms in the contact layer. Assuming that the boundary atoms in the contact layer only contribute 50% of k_{at} , while the interior atoms contribute a full k_{at} , to a very good approximation, the number of boundary atoms is given by $4\left(\sqrt{N_{cont}}-1\right)$, as shown in parentheses in Table 1. Consequently, we have $k_{at} = \frac{k_1}{N_{cont}-2\left(\sqrt{N_{cont}}-1\right)}$. In Table 3, we show the calculated results of k_{at} and γ , as well as the dissipation rate $m\gamma$, for both Pt_{3956} and Pt_{18365} tip apexes.

Given that the critical damping coefficient (γ_c) of the system, according to Eq. (3), is both k and m relevant, i.e., $\gamma_c = 2\sqrt{k/m}$, one can readily show that the damping ratio $\zeta = \gamma/\gamma_c$, a critical measure of the friction state of the system, is independent of the atomic mass of the tip apex, but is now tied to the driving spring stiffness k, given by

$$\zeta = \frac{N_{cont}}{\sqrt{N_{tot}}} \sqrt{\frac{k_{at}}{k}}.$$
 (10)

As shown in Table 3, both Pt₃₉₅₆ and Pt₁₈₃₆₅ tip apexes are *underdamped* when sliding on the Au (111) surface, even

with other relevant parameters for the Pt_{3956} and Pt_{18365} tip apexes in contact with the Au (111) surface

	k _{at} (N/m)	$\gamma (\times 10^{10} \text{ s}^{-1})$	$m\gamma (\times 10^{-11} \text{ kg s}^{-1})$	$\frac{N_{cont}}{\sqrt{N_{tot}}}$	$\sqrt{rac{k_{at}}{k}}$	ζ
Pt ₃₉₅₆	0.575	4.33	5.65	1.032	0.2715	0.2802
Pt ₁₈₃₆₅	0.114	2.89	17.6	3.332	0.1282	0.4270



though the contact layer atoms are close to *critically damped* [15]. As such, it is the damping ratio ζ , that depends not only on the structure property of the tip apex (represented by $\frac{N_{cont}}{\sqrt{N_{lot}}}$), but also on the square root ratio of the lateral stiffness of the individual atoms in the contact layer over the equivalent driving spring stiffness, $(k_a/k)^{1/2}$, a physical–mechanical property of the friction system.

The dependence of the damping ratio on the mechanical pulling system and the atomic number ratio of the tip apex need further discussions. Here, we focus on the effect of k and m of the tip apex on the system damping behavior. First, the apparent correlation between ζ and $1/k^{1/2}$ suggests that if one uses a hard spring to drive the tip apex, friction will likely enter the smooth sliding regime if the combined parameter $\eta = 2E_0\pi^2/ka^2 < 1$ [4, 24, 30]. The reduced damping ratio will likely make the system underdamped in the smooth sliding state. Conversely, if one uses a soft spring to drive the tip apex, the system will tend to enter the stick-slip regime if the combined parameter $\eta = 2E_0\pi^2/ka^2 > 1$, the present case shown in Table 2. Decreasing k (or equivalently increasing the damping ratio ζ , according to Eq. (10)) will also more likely make the system enter into critically damped or even overdamped stick-slip friction regime. At this point, we emphasize that it is the damping ratio ζ , that connects the intrinsic atomic dissipation rate (γ) with the external mechanical driving system (k) through the critical damping coefficient γ_c , which is k and m relevant. Second, increasing the tip apex mass (m) is equivalent to increasing the total number of atoms N_{tot} , therefore, decreasing ζ . According to Eq. (10), the larger N_{tot} will give lower ζ if N_{cont} is kept unchanged, making the system likely underdamped. This situation is consistent with theoretical predictions by Krylov et al. [15] It is therefore intriguing to properly define the tip apex structure to reflect the actual AFM tip apex geometry. The optimized value of $N_{cont}/(N_{tot})^{1/2}$, for a given mechanical driving spring k, will be able to predict the actual stick-slip friction state of the AFM cantilever upon the tip-substrate contact is established.

4.3 Validation of *k*_{cont} and *γ* – Velocity-Dependent Friction Simulations

We show that the contact stiffness and damping derived from the above MD simulations can be readily used in the Langevin Eq. (3) for the PT model. To make the MD simulation and the phenomenological PT modeling for both Pt₃₉₅₆ and Pt₁₈₃₆₅ tip apexes in the same footing, the total masses of the two tip apexes are assumed to have the same 100 Au mass, i.e., $m = 3.29 \times 10^{-23}$ kg. This allows the stick–slip friction to be in the single-slip regime [25]. Velocity-dependent friction simulations are carried out by both MD simulation and Langevin dynamics in the range of V = 0.01 - 1 m/s at

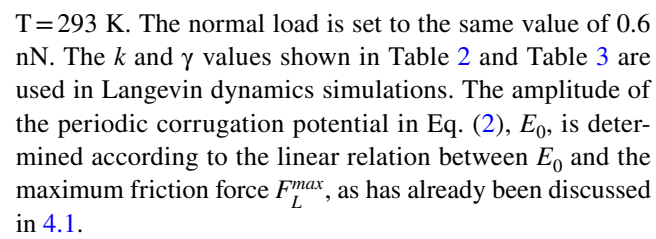


Figure 4 shows the detailed comparisons of the typical stick-slip friction force variations at V=1 m/s and the velocity-dependent mean friction for the two tip apexes. All simulations are carried out by running at least 5 independent simulations to calculate the mean friction forces. We find that MD simulations for the Pt₁₈₃₆₅ tip apex usually take more simulation runs (up to 10 runs) in which any simulation results involving new surface defects generated on the Au (111) surface will be discarded. This scenario may happen when some high energy attached gold atoms experience further diffusion onto the Pt tip apex. The overall remarkable consistency between the MD simulation and the Langevin dynamics modeling, while the latter depends on the properly calculated phenomenological damping coefficient and the contact stiffness from direct MD simulations, validates the general utility of these two parameters in a simple phenomenological modeling.

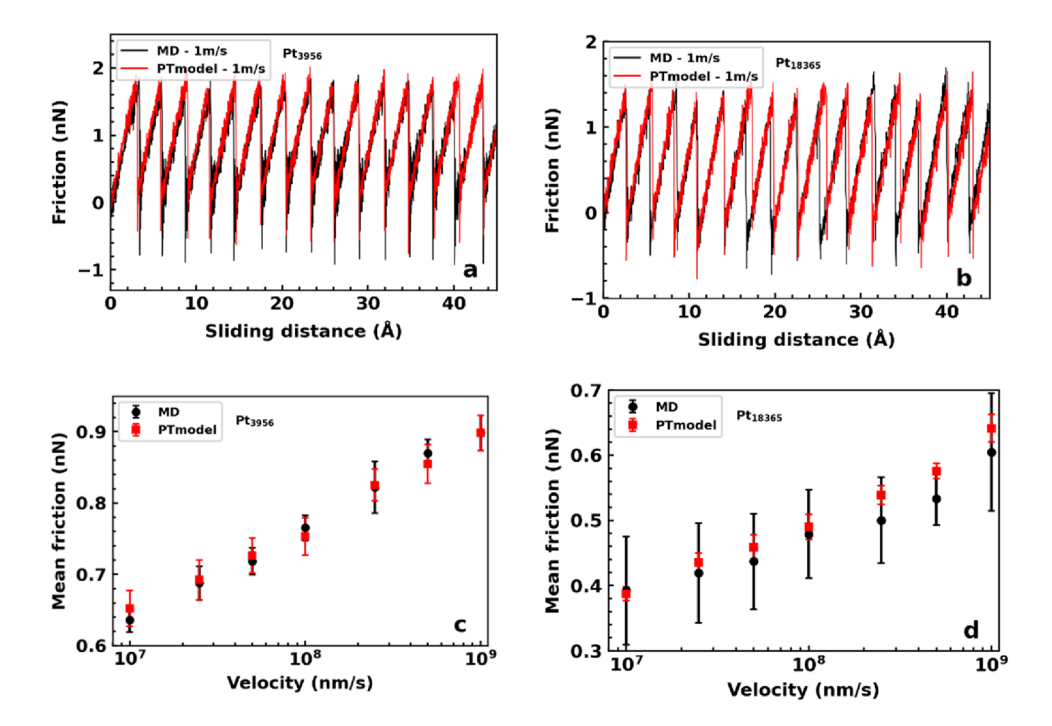
5 Conclusions

We have presented a method of calculating the contact stiffness and damping coefficient necessary for implementing the Prandtl-Tomlinson (PT) model for the study of atomic-scale friction. The two important parameters can be unambiguously determined from straightforward MD simulations if the actual atomic structure of the AFM tip apex is known. We demonstrate that the contact stiffness of the tip-substrate contact k_{cont} , is largely dependent on the very first contact layer atoms in the tip apex, while the damping coefficient γ , is uniquely determined by a combination of the atomic structure of the tip apex and the intrinsic relaxation rate of the individual atoms in the contact layer. In particular, k_{cont} is essentially independent of the temperature and the atomic mass of the AFM tip, and is also less dependent on the normal load if the contact geometry remains unchanged in elastic contact. With these two critical parameters being fully understood and determined, the PT model can reproduce the stick-slip motion of the tip apex predicted by expensive MD simulations. More importantly, a practice of using direct MD simulation to determine k_{cont} and γ brings in a fundamental understanding of the origin of these two parameters in the phenomenological PT model. We emphasize that it is the damping ratio ζ , which connects the intrinsic damping coefficient (γ) of the contact layer with the external mechanical driving system (k), that ultimately determines the friction



Tribology Letters (2024) 72:24 Page 9 of 10 **2**4

Fig. 4 Panels $\bf a$ and $\bf b$ show the variation of the stick–slip friction force versus the sliding distance at V=1 m/s, predicted by the direct MD simulation and the PT Langevin dynamics for both Pt₃₉₅₆ and Pt₁₈₃₆₅ tip apexes. Panels $\bf c$ and $\bf d$ show the velocity-dependent mean friction force versus the sliding speed for the two tip apexes



state of the system. Such an intriguing correlation suggests that, perhaps, given the same dissipation rate γ in the contact layer, the way of energy dissipation should critically depend on the extrinsic behavior of the mechanical driven system, such as its k and m. We anticipate that the method of calculating k_{cont} and γ may find new applications in modeling nanoscale friction in many different systems, and may pave a new revenue to unravel friction dissipation in AFM experimentation.

Author Contributions GZ, RX, YX. and YL performed the research and wrote the main manuscript text. Y. L. finalized the paper. All authors reviewed the manuscript.

Funding This work is supported by the National Science Foundation (NSF 1953171) and the resources of the National Energy Research Scientific Computing Center (NERSC), a DOE Office of Science User Facility supported by the Office of Science of the U.S. Department of Energy under Contract no. DE-AC02-05CH11231.

Data Availability All data relevant to this work will be available upon request after publication of this manuscript.

Declarations

Competing Interests The authors declare no competing interests.

References

 Mate, C.M., McClelland, G.M., Erlandsson, R., Chiang, S.: Atomic-scale friction of a tungsten tip on a graphite surface. Phys. Rev. Lett. 59(17), 1942–1945 (1987)

- Carpick, R.W., Salmeron, M.: Scratching the surface: Fundamental investigations of tribology with atomic force microscopy. Chem. Rev. 97(4), 1163–1194 (1997)
- Gnecco, E., Bennewitz, R., Gyalog, T., Loppacher, C., Bammerlin, M., Meyer, E., Guntherodt, H.J.: Velocity dependence of atomic friction. Phys. Rev. Lett. 84(6), 1172–1175 (2000)
- Vanossi, A., Manini, N., Urbakh, M., Zapperi, S., Tosatti, E.: Colloquium: Modeling friction: From nanoscale to mesoscale. Rev. Mod. Phys. 85(2), 529–552 (2013)
- Krylov, S.Y., Frenken, J.W.M.: The physics of atomic-scale friction: Basic considerations and open questions. Phys. Status Solidi B 251(4), 711–736 (2014)
- Szlufarska, I., Chandross, M., Carpick, R.W.: Recent advances in single-asperity nanotribology. J. Phys. D-Appl. Phys. 41(12), 123001 (2008)
- 7. Li, S., Li, Q., Carpick, R.W., Gumbsch, P., Liu, X.Z., Ding, X., Sun, J., Li, J.: The evolving quality of frictional contact with graphene. Nature **539**(7630), 541–545 (2016)
- Vanossi, A., Bechinger, C., Urbakh, M.: Structural lubricity in soft and hard matter systems. Nat. Commun. 11(1), 4657 (2020)
- Zhang, S., Yao, Q., Chen, L., Jiang, C., Ma, T., Wang, H., Feng, X.-Q., Li, Q.: Dual-Scale Stick-Slip Friction on Graphene/h
 BN Moiré Superlattice Structure. Phys. Rev. Lett. 128(22), 226101 (2022)
- Qu, C., Wang, K., Wang, J., Gongyang, Y., Carpick, R.W., Urbakh, M., Zheng, Q.: Origin of friction in superlubric graphite contacts. Phys. Rev. Lett. 125(12), 126102 (2020)
- Binnig, G., Quate, C.F., Gerber, C.: Atomic force microscope. Phys. Rev. Lett. 56(9), 930–933 (1986)
- Maier, S., Sang, Y., Filleter, T., Grant, M., Bennewitz, R., Gnecco, E., Meyer, E.: Fluctuations and jump dynamics in atomic friction experiments. Phys. Rev. B 72(24), 245418 (2005)
- Krylov, S.Y., Dijksman, J.A., van Loo, W.A., Frenken, J.W.M.: Stick-Slip Motion in Spite of a Slippery Contact: Do We Get What We See in Atomic Friction? *Phys.* Rev. Lett. 97(16), 166103 (2006)



24 Page 10 of 10 Tribology Letters (2024) 72:24

 Abel, D.G., Krylov, S.Y., Frenken, J.W.M.: Evidence for Contact Delocalization in Atomic Scale Friction. Phys. Rev. Lett. 99(16), 166102 (2007)

- van Baarle, D.W., Krylov, S.Y., Beck, M.E.S., Frenken, J.W.M.: On the Non-trivial Origin of Atomic-Scale Patterns in Friction Force Microscopy. Tribol. Lett. 67(1), 15 (2019)
- Li, Q.Y., Dong, Y.L., Perez, D., Martini, A., Carpick, R.W.: Speed Dependence of Atomic Stick-Slip Friction in Optimally Matched Experiments and Molecular Dynamics Simulations. Phys. Rev. Lett. 106(12), 126101 (2011)
- Liu, X.Z., Ye, Z.J., Dong, Y.L., Egberts, P., Carpick, R.W., Martini, A.: Dynamics of Atomic Stick-Slip Friction Examined with Atomic Force Microscopy and Atomistic Simulations at Overlapping Speeds. Phys. Rev. Lett. 114(14), 146102 (2015)
- Gosvami, N.N., Filleter, T., Egberts, P., Bennewitz, R.: Microscopic Friction Studies on Metal Surfaces. Tribol. Lett. 39(1), 19–24 (2010)
- Prandtl, L.: Ein Gedankenmodell zur kinetischen Theorie der festen Körper (A conceptual model to the kinetic theory of the solid body).
 Z. Angew. Math. Mech. 8(2), 85–106 (1928)
- Tomlinson, G.A.: A molecular theory of friction. Philos. Mag. 7(46), 905–939 (1929)
- Dong, Y., Li, Q., Martini, A.: Molecular dynamics simulation of atomic friction: A review and guide. J. Vac. Sci. Technol. A 31(3), 030801 (2013)
- Neumeister, J.M., Ducker, W.A.: Lateral, normal, and longitudinal spring constants of atomic force microscopy cantilevers. Rev. Sci. Instrum. 65(8), 2527–2531 (1994)
- 23. Hu, R., Krylov, S.Y., Frenken, J.W.M.: On the Origin of Frictional Energy Dissipation. Tribol. Lett. **68**(1), 8 (2019)
- 24. Socoliuc, A., Bennewitz, R., Gnecco, E., Meyer, E.: Transition from stick-slip to continuous sliding in atomic friction: entering

- a new regime of ultralow friction. Phys. Rev. Lett. **92**(13), 134301 (2004)
- Xu, R.-G., Zhang, G., Xiang, Y., Garcia, J., Leng, Y.: Will polycrystalline platinum tip sliding on a gold(111) surface produce regular stick-slip friction? Langmuir 38(22), 6808–6816 (2022)
- Voter, A. F.: Embedded Atom Method Potentials for seven FCC metals: Ni, Pd, Pt, Cu, Ag, Au, and Al. Los Alamos Unclassified Technical Report # LA-UR. 93–3901 (1993).
- Plimpton, S.: Fast parallel algorithms for short-range moleculardynamics. J. Comput. Phys. 117(1), 1–19 (1995)
- Thompson, A.P., Aktulga, H.M., Berger, R., Bolintineanu, D.S., Brown, W.M., Crozier, P.S., in 't Veld, P. J., Kohlmeyer, A., Moore, S. G., Nguyen, T. D., Shan, R., Stevens, M. J., Tranchida, J., Trott, C., Plimpton, S. J.: LAMMPS - a flexible simulation tool for particle-based materials modeling at the atomic, meso, and continuum scales. Comput. Phys. Commun. 271, 108171 (2022)
- Allen, M.P., Tildesley, D.J.: Computer Simulation of Liquids. Clarendon Press, Oxford (1987)
- Medyanik, S.N., Liu, W.K., Sung, I.-H., Carpick, R.W.: Predictions and observations of multiple slip modes in atomic-scale friction. Phys. Rev. Lett. 97(13), 136106 (2006)

Publisher's Note Springer Nature remains neutral with regard to jurisdictional claims in published maps and institutional affiliations.

Springer Nature or its licensor (e.g. a society or other partner) holds exclusive rights to this article under a publishing agreement with the author(s) or other rightsholder(s); author self-archiving of the accepted manuscript version of this article is solely governed by the terms of such publishing agreement and applicable law.

